Lawrence Berkeley Laboratory
UNIVERSITY OF CALIFORNIA

Engineering & Technical Services Division

Presented at the IEEE Nuclear Science Symposium, San Francisco, CA, October 19-21, 1983; and to be published in IEEE Transactions on Nuclear Science

SEMICONDUCTOR DETECTORS AND DOUBLE BETA DECAY

F.S. Goulding, D.A. Landis, P.N. Luke, N.W. Madden, D.F. Malone, R.H. Pehl, and A.R. Smith

November 1983

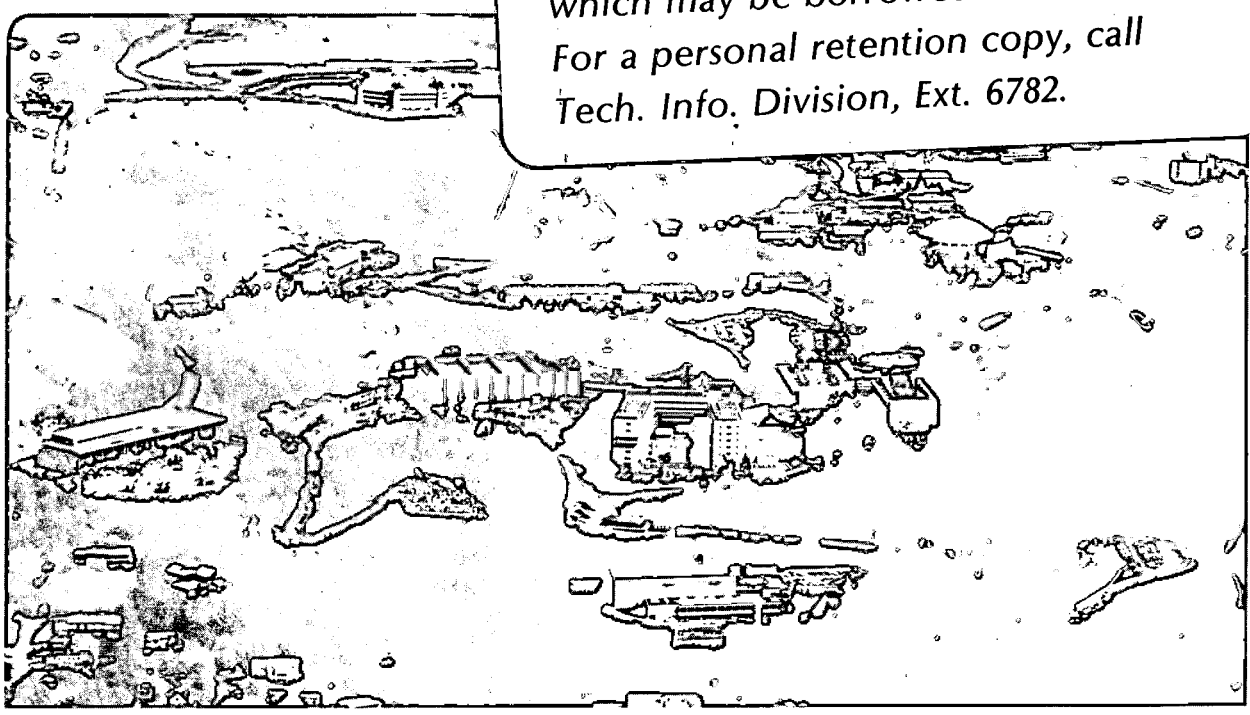

Prepared for the U.S. Department of Energy under Contract DE-AC03-76SF00098

DISCLAIMER

SEMICONDUCTOR DETECTORS AND DOUBLE BETA DECAY

LBL-16682

F.S. Goulding, D.A. Landis, P.N. Luke, N.W. Madden, D.F. Malone,
R.H. Pehl, and A.R. Smith

Lawrence Berkeley Laboratory
University of California
Berkeley, CA 94720 USA

I. Introduction

This paper is aimed at an audience of semiconductor detector makers and those interested in the science and applications of these detectors. Those of us fortunate enough to have been members of this community in the 1960's recognize the unique contributions made by our detector art to the unravelling of nuclear structure. Since that time, germanium detectors have continued to play a vital role in a wide variety of research applications both in the laboratory and in space, and have also assumed a practical role in monitoring applications, in such areas as well-logging and resource exploration, and in a broad range of practical applications such as activation analysis. Silicon detectors have followed a parallel path, with initial research applications being followed by large scale application to x-ray fluorescence analysis. Based on these practical applications, a large industry has grown and prospered.

A very important research application for these detectors has now come to light. Theoretical physicists have devoted great effort in developing an adequate theory to link three of the four forces of nature (weak, electromagnetic and strong forces). This work has produced Grand Unified Theories (GUT) which must stand the test of experiments. There also has been considerable discussion concerning the "missing mass" in the universe, whether adequate mass exists in the universe to make it closed (i.e., it will eventually collapse) or open (i.e., infinitely expanding). Recent theoretical studies and observations of the stability of galaxies have strongly indicated the presence of large amounts of invisible mass in these objects. One element in the uncertainty associated with the missing mass is the question whether the neutrino has rest mass. These two questions are among the most important in physics today. A better understanding of the nature of the neutrino could provide desired answers. This paper will discuss the underlying theory and a germanium detector experiment which could make a striking contribution to the resolution of these questions.

II. Double Beta Decay

Before discussing the phenomenon of $\beta\beta$ decay a few words about normal (single) beta decay are in order. The emission by a nucleus of a single electron accompanied by an electron antineutrino (usually given the symbol $\overline{\nu}_e$) is a well known process that is thoroughly understood theoretically. The process involves conversion of a neutron in the nucleus to a proton with a change of +1 in the charge Z of the nucleus. Sharing of energy between the electron (β^- particle) and the neutrino results in a distribution of electron energies having the shape described by the Fermi theory. The end point energy corresponds to the change in mass involved in restructuring the nucleus and creating the electron. Thus, for example, ^{32}P (mass excess -24.303 MeV) decays by emission of an electron whose end point energy is 1.710 MeV, forming ^{32}S (mass excess -26.013 MeV). The end point energy and the shape of the energy distribution in its vicinity is sensitive to neutrino mass and measurement of this shape is being exploited to determine the neutrino mass.

For β decay to occur, the daughter nucleus (e.g., ^{32}S) must be more tightly bound than the parent (e.g., ^{32}P). The decay rate (and therefore the half life of the parent nucleus) depends on the energy involved in the transition, on the matrix elements for the two nuclei and on quantum number selection rules. For our present purpose, we emphasize that the transition must be energetically possible.

For reasons that will become evident as we proceed, we illustrate in Fig. 1 a small region of the Chart of the Nuclides in the region $Z \sim 32$ and atomic weight $A \sim 76$. In this diagram, stable nuclides are shown shaded. Beta decay proceeds along diagonal lines from bottom right to top left. Positron emission or electron capture causes the opposite movement. Nuclear theory permits calculation of the binding-energy of various combinations of protons and neutrons that constitute nuclei. Figure 2 shows the calculated binding energy parabolas for atomic weights A = 74, 75 and 76. As stated earlier, nuclear transitions are only energetically possible where the final nucleus is more tightly bound than its parent. For example, looking at the A = 74 curves, ^{74}Ga can decay by β^- (electron) emission to ^{74}Ge and ^{74}As can decay by β^+ (positron) emission to ^{74}Ge, the most stable nucleus for A = 74. The total energy released in kinetic energy of the β^- and β^+ particles and corresponding neutrinos and in γ emission from the excited daughter nuclei is determined by the energy differences indicated in Fig. 2.

For our present purpose, the most interesting aspect of Fig. 2 is the situation occurring in the case of ^{76}Ge. The A = 76 curve shows that the decay of ^{76}Ge to ^{76}As is not energetically possible because ^{76}Ge is about 0.9 MeV more tightly bound than ^{76}As. Since nuclei containing even numbers of neutrons and protons (even-even) are more tightly bound than odd-odd nuclei, the double curves for A = 74 and A = 76 result. Note that ^{76}Se is more tightly bound (by about 2 MeV) than ^{76}Ge. Therefore, a transition involving emission of two electrons by a ^{76}Ge nucleus to form a ^{76}Se nucleus is energetically possible. While other considerations may make such a transition highly improbable, this energetically possible event, if observed, will provide a major breakthrough in understanding our universe. As is common in physics, observation of a very rare and improbable process may be a key to our understanding of nature.

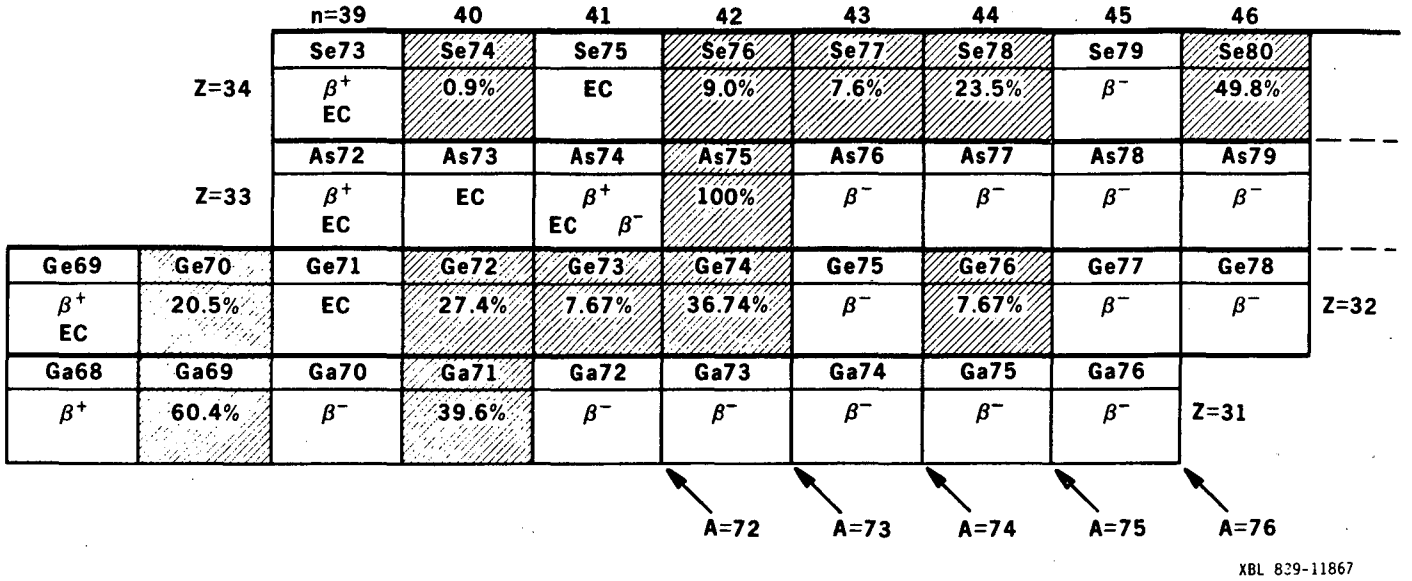

Fig. 1: Simplified Chart of the Nuclides for the region of ^{76}Ge. Stable nuclides are shaded.

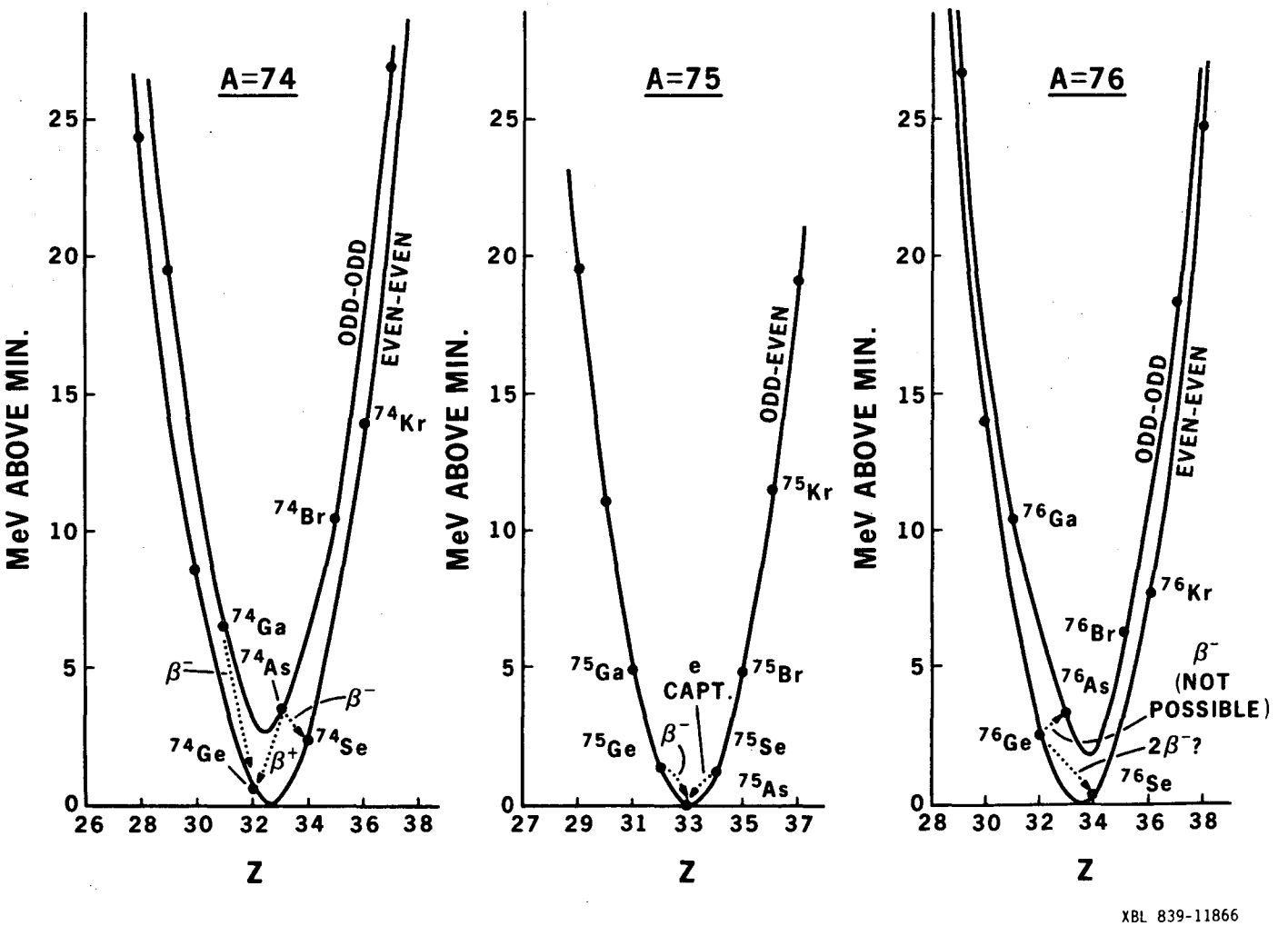

Fig. 2: Binding energy plots for nuclides near ^{76}Ge. Note that energy considerations permit ββ decay of ^{76}Ge to ^{76}Se.

Table 1: Potential Double-Beta Decay Nuclei

Transition	A	Z	Abundance(%)	Energy	Single-Beta Energy
Ca - Ti	46	20	.003	.985	-1.38
Ca - Ti	48	20	.185	4.267	+0.289
Zn - Ge	70	30	.62	1.008	-0.653
Ge - Se	76	32	7.67	2.041	-0.923
Se - Kr	80	34	49.82	0.138	-1.871
Se - Kr	82	34	9.19	3.003	-0.089
Kr - Sr	86	36	17.37	1.240	-0.054
Zr - Mo	94	40	17.40	1.230	-0.921
Zr - Mo	96	40	2.80	3.364	+0.215
Mo - Ru	100	42	9.62	3.034	-0.335
Ru - Pd	104	44	18.70	1.321	-1.145
Pd - Cd	110	46	11.80	2.004	-0.868
Cd - Sn	114	48	28.86	0.547	-1.439
Cd - Sn	116	48	7.58	2.811	-0.517
Sn - Te	122	50	4.71	0.349	-1.622
Sn - Te	124	50	5.98	2.263	-0.653
Te - Xe	128	52	31.79	0.872	-1.268
Te - Xe	130	52	34.49	2.543	-0.407
Xe - Ba	134	54	10.44	0.731	-1.328
Xe - Ba	136	54	8.87	2.718	-0.112
Ce - Nd	142	58	11.07	1.379	-0.777
Nd - Sm	148	60	5.71	1.936	-0.514
Nd - Sm	150	60	5.60	3.390	-0.036
Sm - Gd	154	62	22.61	1.260	-0.718
Gd - Dy	160	64	21.75	1.782	-0.029
U - Pu	238	92	99.28	1.173	-0.117

We have described ββ decay in terms of one nuclide (^{76}Ge); the same process is energetically possible in other nuclides. Table I lists these cases and the transition energies involved. Also listed are the single β-decay energy differences for these nuclides--in all cases but two these energy differences are negative, so single β decay cannot compete with ββ decay. Because ^{76}Ge constitutes almost 8% of germanium, internal counting in germanium detectors provides a particularly attractive way to detect ββ decay. However, this does not mean that clever techniques using other candidate nuclides cannot be employed. We will see that such techniques have been used and that it is by such methods that initial experimental indications of ββ decay have been obtained.

III. Detailed Picture of Double Beta Decay

Our discussion so far has only shown that ββ decay is energetically possible in nuclides such as ^{76}Ge. We also know from Fig. 2 and Table 1 that slightly over 2 MeV should be released when ^{76}Ge converts to ^{76}Se. Two very different mechanisms are possible for emission of the electrons in this process. In the first case, the emission of the two electrons can be accompanied by emission of two electron antineutrinos. Thus:

$$^{76}\text{Ge} \longrightarrow {}^{76}\text{Se} + 2\,e^- + 2\,\bar{\nu}_e \quad (+2.041\ \text{MeV})$$

As in single β decay, energy is shared between the electrons and neutrinos so the sum of the electron energies will show a continuous distribution from zero to about 2 MeV--as shown in the continuous distribution of Fig. 3. A very different case occurs if the two electrons are emitted with no neutrinos.

$$^{76}\text{Ge} \longrightarrow {}^{76}\text{Se} + 2\bar{e} \quad (+\ 2.041\ \text{MeV})$$

In this case the sharp line spectrum shown in Fig. 3 results. If the first excited 2^+ level of ^{76}Se is populated, the line at 2.041 MeV will be weaker and a second line at 1.482 MeV will be present. A gamma ray of 559 keV will be produced (virtually at the same time) as the ^{76}Se de-excites to the 0^+ ground state.

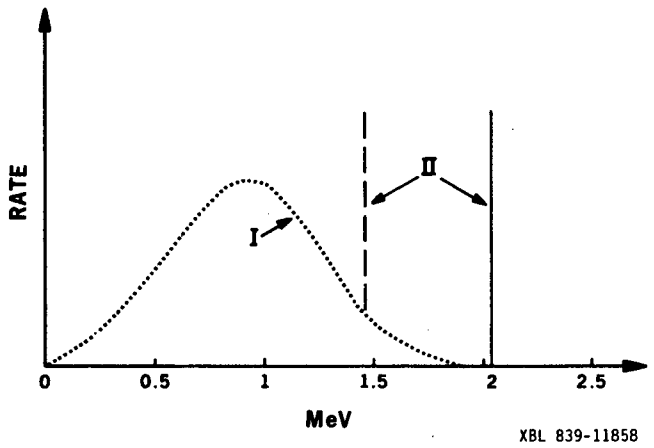

Fig. 3: Energy distribution (summed for both electrons) in the ββ decay of ^{76}Ge. The continuous distribution (I) involves the emission of two neutrinos. The lines at 2.041 MeV and 1.482 MeV are due to neutrinoless ββ decay (0^+ to 0^+ and 0^+ to 2^+ transitions respectively).

While observation of the first mechanism (I) is important, attention is focused primarily on the neutrinoless mechanism (II). Whereas mechanism I produces 2 electrons and 2 antiparticles ($\bar{\nu}_e$), mechanism II creates 2 electrons and no antiparticles, changing the lepton number by 2. Observation of neutrinoless ββ decay would be the first experimental observation of a nuclear process in which leptons are not conserved. Non-conservation of leptons is suspected as a result of Grand Unified Theories and its observation would be an important check of these theories.

Mechanism II involves theoretical concepts that are beyond the scope of this paper but the general nature of the theory can reasonably be discussed in terms of Fig. 4. Here we picture two neutrons decaying by weak interactions to produce two protons, two electrons and neutrinos $\bar{\nu}_e'$ and $\bar{\nu}_e''$. If the two neutrinos escape from the nucleus, the process is ββ decay with the emission of two neutrinos. However, if the first neutrino $\bar{\nu}_e'$ can be absorbed by the second neutron and, in some manner, behave like the emission of neutrino $\bar{\nu}_e''$, no neutrinos escape and neutrinoless ββ decay results. Certain conditions about the neutrino must be met for this to occur:

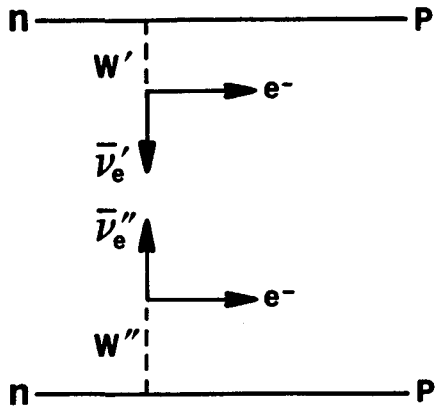

XBL 839-11855

Fig. 4: Simple model for ββ decay process.

(i) The neutrinos involved must be of the Majorana type as distinct from the Dirac type (i.e. the particle and its antiparticle must be identical, and not opposites as in the Dirac case--such as positrons and electrons)

and

(ii) One of the following conditions must be satisfied:

a) The neutrinos must have mass, or
b) The normal left-handed chirality of the neutrino breaks down and a small right-handed admixture is present.
c) A mixture of a) and b).

Assuming that these conditions are met, the probability of neutrinoless ββ decay depends on the value of the neutrino mass and/or the right-handed admixture, on the energy available for the transition, and on the matrix elements of the parent and daughter nuclei. The rate of neutrinoless ββ decay is highly dependent on the transition energy (rate $\propto E^5$). This greatly favors study of the cases in Table I where large energy differences exist. Assuming that the admixture of right-handed chirality is zero, the rate of the process will be proportional to the square of the neutrino mass. Separating the effects of neutrino mass from the admixture of right-handed chirality in the normally left-handed neutrinos is difficult. If we represent the neutrino mass by m_ν and the fraction of the right-handed chirality as η, a measurement of decay half life can be interpreted as possible combinations of m_ν and η as shown in Fig. 5. Similar plots can be made for different cases and observed half lives. Theory predicts that the ratio of intensities of the 2.041 MeV and 1.482 MeV lines can be used to distinguish between the effects of neutrino mass and the admixture of right-handed chirality. The 0^+ to 0^+ transition can result from neutrino mass or from a right-handed chirality admixture, whereas the 0^+ to 2^+ transition can only proceed if the right-handed admixture exists. The ratio of (0^+ to 0^+) to (0^+ to 2^+) transitions, if determined, can pinpoint the actual values of m_ν and η.

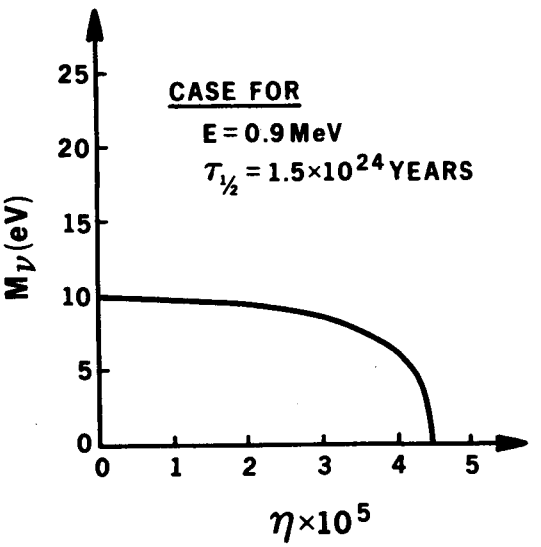

XBL 839-11857

Fig. 5: Typical case of permitted values of neutrino mass m_ν and the right-handed chirality fraction η established by a neutrinoless ββ decay half-life measurement.

As indicated, these theoretical aspects are very complex and further explanation is beyond the scope of this paper. Therefore, we will focus on the experimental difficulties and the techniques that have been and are being developed to handle the major problems. In keeping with our interest in semiconductor detectors, we will focus on ^{76}Ge which may decay to ^{76}Se with an energy release of 2.041 MeV. For this transition, the neutrinoless ββ decay half life will be 10^{24} years if the neutrino mass is 1 eV and if no right-handed chirality admixture is present. The following observations should be made about neutrino mass and its experimental consequences:

(i) Russian experiments, using a β-ray spectrometer to measure the energy distribution of electrons near the endpoint of the β^- spectrum from tritium decay, suggest that the neutrino mass exceeds 15 eV. Uncertainty about details of the energy absorbing processes in the source casts doubt on these measurements. Since this method does not discriminate between Dirac and Majorana neutrinos, such a result is not in total conflict with some ββ decay measurements that indicate that m_ν must be smaller than 10 eV.

(ii) From an astrophysical point of view the neutrino mass range from about 1 to 30 eV is particularly interesting. This corresponds to a ^{76}Ge half-life range of about 10^{24} to 10^{21} years.

(iii) For 1 kg of natural germanium, a half life of 10^{24} years corresponds to approximately 0.5 disintegrations/year.

IV. Experimental Observations of Double Beta Decay

The extremely small decay rates present grave difficulties in discriminating between real decays and background events. Two basic approaches have been adopted to overcome the problem. The first involves the use of very long accumulation times (a significant fraction of the age of the earth) and consists of detecting the daughter products of a $\beta\beta$ decay process accumulated in rocks over a very long time. The second method is to design highly selective spectroscopic counting systems in which individual decays can be detected. This paper will focus on the latter method but it is of interest to glance at results from the geochemical experiments.

A. Geochemical Measurements

For the geochemical method to be effective, the age of the ore must be well established, a high content of the parent nuclide must be present, retention of the daughter product in the ore must be plausible and sensitive techniques such as mass spectrometry must be used to measure the isotopic ratios of parent and daughter. Furthermore, all potential sources of error, such as background or other potential means of production of the daughter (e.g., by solar neutrino absorption) must be carefully assessed. A number of measurements that meet these criteria have been made on ores with ages ranging from 10^7 to 10^9 years from many parts of the world. The transitions $^{130}Te \longrightarrow {}^{130}Xe$, $^{128}Te \longrightarrow {}^{128}Xe$ and $^{82}Se \longrightarrow {}^{82}Kr$ have been studied by these methods. On the basis of these results, half lives in the 10^{20} to 10^{21} year range have been calculated for the $^{130}Te \longrightarrow {}^{130}Xe$ and $^{82}Se \longrightarrow {}^{82}Kr$ transitions where the energies are high (2.5 to 3 MeV). At high energies the two-neutrino process is greatly favored over the no neutrino process; therefore, these results indicate half lives of 10^{20} to 10^{21} years for two-neutrino decay.

Attempts have been made to establish unequivocally the existence of the neutrinoless decay mode using geochemical techniques. These attempts are based on comparison of the daughter products in the $^{130}Te \longrightarrow {}^{130}Xe$ and $^{128}Te \longrightarrow {}^{128}Xe$ decays whose transition energies are very different (2.54 MeV and 0.87 MeV, respectively). Since theory predicts a E^5 dependence of decay rate for neutrinoless decay and an E^{11} dependence for the two-neutrino process, the $^{130}Te \longrightarrow {}^{130}Xe$ decay is dominated by the two-neutrino process, while the no-neutrino process is favored for the $^{128}Te \longrightarrow {}^{128}Xe$ decay. The results of these experiments are inconclusive, but, interestingly, the half life of the $^{128}Te \longrightarrow {}^{128}Xe$ decay process has been established to be greater than 8×10^{24} years, a number that demonstrates how difficult direct counting experiments are.

B. Direct Decay Observations

Direct detection experiments are aimed at observing individual decays and characterizing electron energies and other relevant parameters to distinguish between neutrinoless $\beta\beta$ decay events and background. These experiments are usually classified primarily in terms of the nuclei studied. Many experiments involve the use of separated or partially separated isotopes to increase the "activity" while minimizing internal absorption in the sample. In principle, we could grow germanium crystals from separated ^{76}Ge and then fabricate detectors from these enriched crystals but the cost of such detectors would be prohibitive.

(i) Non-^{76}Ge Experiments: The detectors employed or planned in these experiments include spark chambers, cloud chambers, scintillators, time projection chambers and large area silicon detectors. Active background rejection shielding and/or passive lead or mercury shielding are used in most cases, and efforts are made to perform identification of the β-particles by energy measurement, by bending in a magnetic field and/or by tracking.

Present results using these methods have been negative (i.e., neutrinoless $\beta\beta$ decay was not observed at the detection limit) so only limiting values can be assigned to m_ν and η. An experiment by Moe and Lowenthal studying the decay $^{82}Se \longrightarrow {}^{82}Kr + 2e^-(3\ MeV)$ in a cloud chamber surrounded by trigger and background rejection chambers observed the two-neutrino $\beta\beta$ decay with a half life of approximately 10^{19} years. This is one to two orders of magnitude shorter than the geochemical result for the same decay process.

One of the intriguing experiments planned (Irvine-Moe) uses a gas-filled time projection chamber (TPC) to observe the decay of ^{82}Se while another group (Irvine-Chen) plans to construct a liquid Xe TPC to observe the decay of ^{136}Xe. ^{136}Xe is a very attractive parent nucleus for use in detector experiments.

(ii) Internal ^{76}Ge Decay Detection in Ge Detectors: This approach is particularly attractive for several reasons. The $^{76}Ge \longrightarrow {}^{76}Se$ transition energy is reasonably high (2.041 MeV) so the half life may not be too long to measure. In the absence of right-handed chirality, the half life will be approximately 10^{24} years for a neutrino mass of 1 eV and 10^{22} years for 10 eV. Furthermore, the abundance of ^{76}Ge in natural germanium is moderately high (7.67%). As indicated earlier, 10^{24} years corresponds to 0.5 counts/year in 1 kg of natural germanium. While this rate is very low, the ability of germanium detectors to achieve an energy resolution close to 0.1 at 2 MeV is of great value in rejecting background.

These features led to germanium detector experiments by the Milano (Fiorini) group starting in the early 1970's. Results obtained by this group have provided the basis for all later efforts and, at this time, their experiments in the Mont Blanc tunnel have established the longest half-life limits for neutrinoless decay. These limits are now $> 2.3 \times 10^{22}$ years for the 0^+ to 0^+ transition and $> 8.7 \times 10^{21}$ years for the 0^+ to 2^+ transition. A similar limit has been obtained by the Battelle-South Carolina group for the 0^+ to 0^+ transition and a Bordeaux-Zaragoza group has obtained a limit of $\sim 2 \times 10^{21}$ years for the 0^+ to 2^+ transition. Other groups at Caltech, Guelph-Aptec and elsewhere are presently performing similar experiments. The neutrino mass limit established by these half-life limits is < 10 eV which is substantially smaller than the Russian results using ^3H β decay. As indicated earlier, questions regarding the validity of the Russian results together with the possibility that the neutrino may be a Dirac particle reduce the weight given to this discrepancy.

These experiments use about 125 cm^3 germanium detectors (about 600 gm of germanium) and counting

periods in the 100 to 200 day range. However, they differ in other details. The Milano group does not use an active background rejection shield; the Battelle-South Carolina group has used such a shield in some experiments and the Bordeaux-Zaragoza group has used such a shield both for background rejection and for detection of the 559 keV γ rays emitted by deexcitation of the ^{76}Se nuclei from their first excited state to their ground state.

The similarity among these "first generation" ^{76}Ge experiments leads us to discuss only the Milano group system that has evolved over a period of about 12 years. This work is the foundation for the "second generation" experiments being prepared--one of which will be described in some detail in the next section.

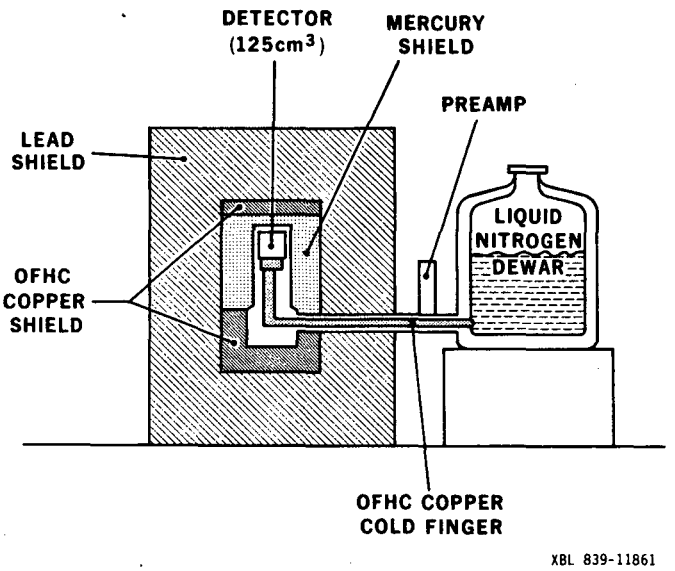

Fig. 6: Schematic drawing of the Milano group germanium detector system used for ^{76}Ge $\beta\beta$ decay experiments.

Figure 6 shows a cross-sectional view of the detector system being used by the Milano group at the present time. A lithium-drifted 125 cm^3 germanium detector is mounted in a holder made mainly of 0.5 mm thick OFHC (Oxygen-Free High Conductivity) copper within a 1 mm thick titanium cap. In early work the shield consisted of 5 cm of OFHC copper and 20 cm of lead. In later experiments, most of the copper shield was replaced by 4.5 cm thick triply distilled mercury as shown in Fig. 6. As discussed in more detail in the next section, background in these experiments is caused partly by natural uranium and thorium activities in materials and partly by cosmic-ray interactions. The Milano group uses selected cryostat materials to reduce uranium and thorium activities and ~ 1800 meters of rock above the Mont Blanc tunnel to shield from cosmic rays. Their background results, shown in Fig. 7, have often formed the basis for the design of later experimental systems. Figures 8a and 8b show the spectra obtained in the vicinity of the 0^+ to 0^+ and 0^+ to 2^+ transitions after a counting time of nearly 4500 hours.

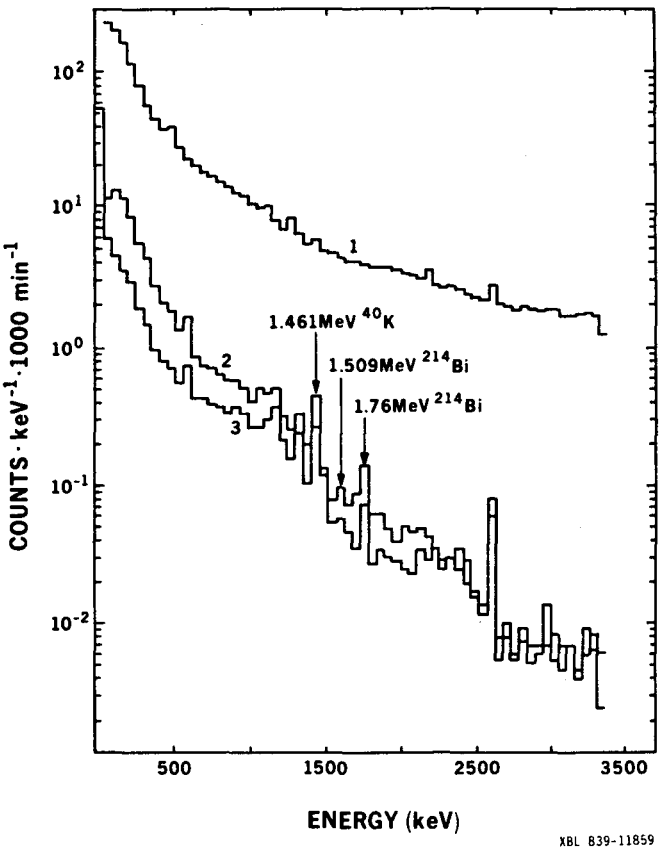

Fig. 7: Backgrounds observed in the Milano group experiments. Curve 1 is the result above ground; Curves 2 and 3 show the underground results with Cu and Hg shields.

The following conclusions can be drawn by analysis of Figs. 7 and 8:

- In the absence of an active shield at ground level, background produced by cosmic rays is completely dominant. In the energy region of interest, a background reduction factor of two orders of magnitude results from virtual removal of cosmic rays.
- A slight further improvement in background results from replacement of a large part of the OFHC copper shield by triply distilled mercury--despite the fact that the copper was selected for low natural activity.
- In the 2-MeV region the background is in the range of 2 to 3 x 10^{-2} counts/keV/1000 min. Expressed in more appropriate units, this corresponds to about 15 counts/keV/year or roughly 40 counts/year in the expected γ-ray peak width of 3 keV at 2 MeV. The RMS fluctuation in this number would be ~6 counts/year, giving a 2σ value of about 15 counts/year. In the ~ 600 gm of germanium contained in this detector system, a half life for neutrinoless $\beta\beta$ decay of 10^{22} years (equivalent to m_ν = 10 eV if no right-handed chirality is present) would produce about 30 decay events/year. Therefore, the measurable half life limit with this system in one year of counting

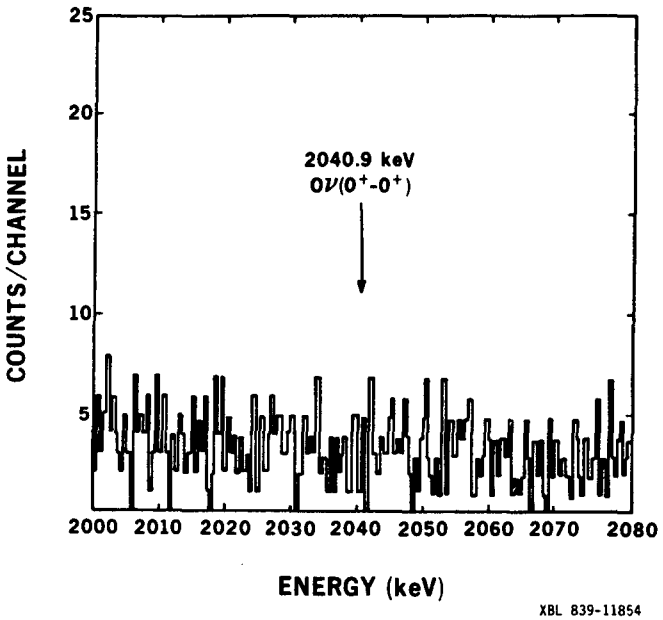

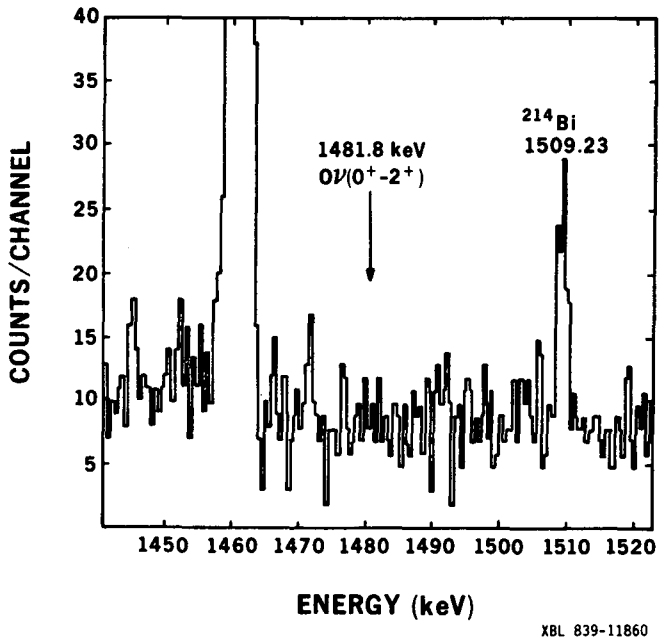

Fig. 8: a) Latest published Milano group spectrum for the 0^+ to 0^+ (2.041 MeV) transition
b) Latest spectrum for the 0^+ to 2^+ (1.482 MeV) transition.
(a) and (b) represent almost 4500 hours of counting.

will be slightly more than 10^{22} years and the maximum mass of a Majorana neutrino can be established as slightly less than 10 eV. As the counting time Tc is increased, the background fluctuations increase as $Tc^{1/2}$ while the decay events increase linearly. Therefore, the half life limit that can be set will increase as $Tc^{1/2}$. Because the half life is proportional to $1/m_\nu^2$ the limit on m_ν will only decrease as $Tc^{-1/4}$. In other words, increasing the counting time by a factor of 10 (to 10 years) will only set the m_ν limit at about 5 eV.

- Background in the 1.5 MeV region of the 0^+ to 2^+ transition is roughly twice that at 2 MeV, so the limit on the half life for this transition is approximately two times shorter than for the 0^+ to 0^+ transition.

These conclusions illustrate the extreme difficulties in placing a small limit on m_ν unless more decays can be observed and the background reduced. In the second generation experiments to be discussed in the next section, detector systems with more than 10 times the amount of germanium used in the Milano group's experiment are planned. Clearly, much more emphasis must also be placed on reducing background.

V. Planned Second Generation ^{76}Ge Experiments

A number of groups are planning substantially expanded ^{76}Ge detector experiments. These include the Battelle-South Carolina, Bordeaux-Zaragoza, Milano, Caltech and Guelph-Aptec groups. Perhaps the most advanced of these new systems is being developed and fabricated in our laboratory at LBL in collaboration with a UC Santa Barbara group. The remainder of this paper will be devoted to a discussion of the design and physics considerations involved in this system and of some of the very special fabrication techniques being employed.

Fortunately, this class of particle physics experiments does not involve teams of 50+ people; nevertheless, our group is substantial in size and each person is bringing special talents into the project. The people involved are:

LBL: F.S. Goulding, D.A. Landis, P.N. Luke, N.W. Madden, D.F. Malone, R.H. Pehl, and A.R. Smith

UCSB: D. Caldwell, D. Grumm, R. Eisberg, D. Hale, M. Witherell

A. General System Description

The first consideration in the design of the experiment must be the amount and distribution of germanium used in the detector systems. This must be conditioned by practical factors such as cost and availability of detectors, by detector system fabrication experience and by physical constraints involved in the background rejection system. A design (see Figs. 9, 10) was chosen that involves clustering eight germanium detectors each 5.5 cm diameter x 7 cm length (vol = 150 cm^3) in a tightly packed volume roughly 6" x 6" x 9" in size. This volume is then surrounded by a 6" thick wall of NaI(Tl) scintillators consisting of 10 individual scintillators. Outside this scintillator shield, a 2" space exists that will be filled with additional low activity γ-ray shielding material, neutron moderator/absorber material, or a combination of both; the final choice to be determined by initial tests on the assembly. Finally, a 6" thick low activity lead shield surrounds the whole assembly. The total weight of the assembly is in excess of seven tons and most of the scintillators weigh about 100 lbs each. A presently undefined plastic scintillator cosmic ray shield will surround the assembly in the initial experiments to be carried out soon in the low-background counting facility at LBL. We anticipate operation in an underground facility sometime in 1985.

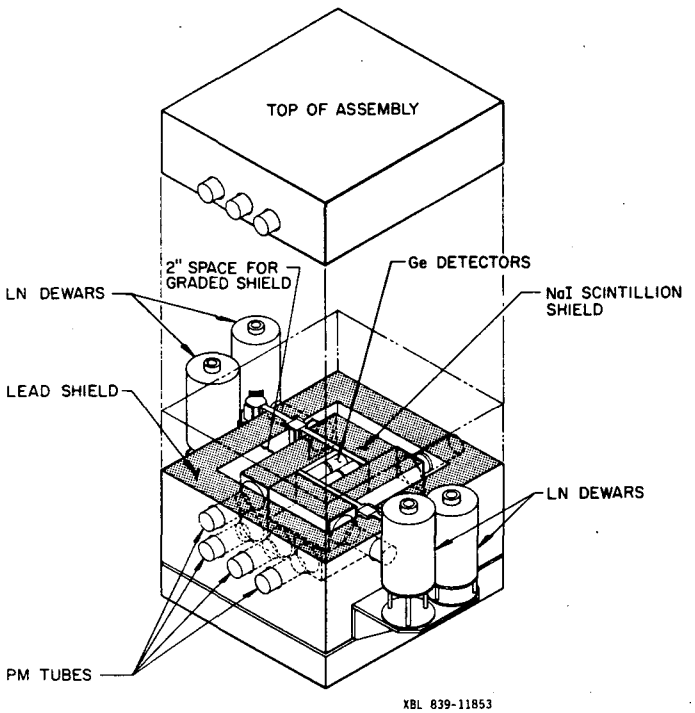

Fig. 9: Cut away drawing of complete LBL/UCSB $\beta\beta$ decay system.

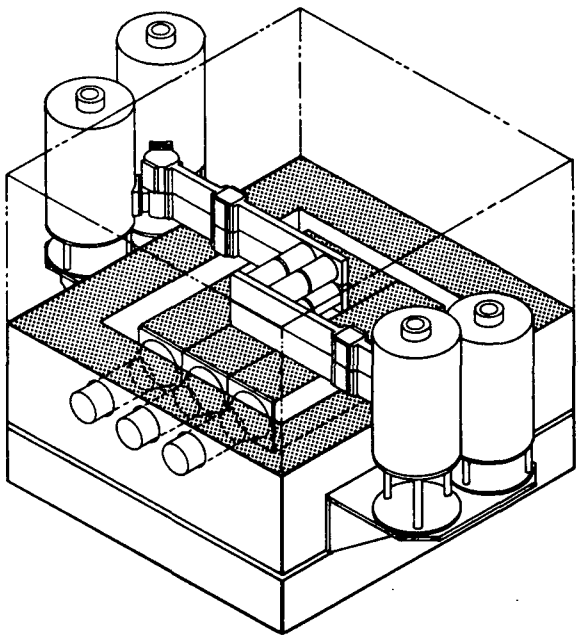

Fig. 10: View of the LBL/UCSB system with all but the bottom layer of scintillator shield removed.

The germanium detectors have been produced by Ortec and will be mounted at LBL in specially designed cryostats. We have chosen to mount two detectors in each of four cryostats. This was judged to be the optimum compromise in regard to ease of detector mounting, system reliability and performance. The cryostat and detector mounting arrangement is designed to minimize material (all specially selected for low background) that would reduce the transmission of γ rays scattered from Ge detectors into the NaI shield. The smallest possible holes in the NaI shield must be employed for entry of the cold fingers and the germanium detectors must not be in the direct line of view through these holes.

Low activity materials have been selected for all components with particular emphasis on those in the counting chamber. The NaI scintillators are canned in OFHC copper with only a 0.25 mm wall thickness facing the counting chamber. We draw attention to the fact that canning the NaI crystals involves many items, each of which must be individually checked for activity (involving several days of counting of a large sample of each material in very low background scintillation and germanium detector systems). Materials checked in this way included the foam rubber normally used at one end of the crystal, the quartz windows used at the opposite end, the white reflector paper used to surround the crystal, the copper used to can the crystals and the epoxy adhesives employed. The phototubes, light pipes, magnetic and light shields were also selected and tested before use. Fiberglass laminates and some electronic components used in the phototube base in the initial design were found to contain as much activity as the phototubes; although they are well removed and shielded, we intend to replace these parts later.

The electronics consist of power supplies, preamplifiers, amplifiers and digitizers and an interface to an HP9835 computer that will acquire all data, control the operation of the system and perform routine calibrations using sources introduced via a "rabbit" (nylon tube) into the center of the system. These calibrations, performed at regular intervals, will check all energy scales, thereby permitting correction of data for any small slow gain drifts. Any event that meets certain "trigger" requirements will be fully characterized in terms of detector signals, pulse shapes and time of occurrence and a record of the event will be written onto a Winchester disk. Histograms of certain types of events will also be accumulated on-line to permit immediate analysis and to provide a rather complete check on system operation. However, the main non-calibration data analysis will be performed off-line on a highly selected group of events characterized basically by the following criteria:

(i) A count occurs in a single germanium detector with no accompanying event in NaI or germanium detectors (0^+ to 0^+ candidate). This will not distinguish a 0^+ to 0^+ candidate from a 0^+ to 2^+ candidate if the 559 keV γ ray produced as the ^{76}Se de-excites from the first excited state to the ground state is absorbed in the same germanium detector.

(ii) A count in a single germanium detector with an accompanying energy deposition of 559 keV in another detector (0^+ to 2^+ candidate).

The design of the system and the associated electronics is predicated on the assumption that the experiment may be required to run in an underground facility for a period of several years. Therefore, fully automatic operation with only occasional attention from experimental staff is considered essential.

B. Special Mechanical Design and Fabrication Features

An essential aspect of the design of this system is that Compton scattered or annihilation γ rays

leaving a germanium detector have a very high probability of being detected in the NaI shield or in another germanium detector. If this is achieved, events due to the $\beta\beta$ decay, which deposit energy in a small region (~ 1 mm) inside the detector, can be distinguished from high-energy γ rays (> 2.041 MeV) that Compton scatter in the detector leaving the same amount of energy as the $\beta\beta$ decay events. We also want to detect the escape of 559 keV γ rays from the germanium detectors because these may be used as a label for 0^+ to 2^+ $\beta\beta$ decay events.

These requirements mean that the NaI shield should be thick enough to have virtually 100% efficiency for detection of Compton scattered γ rays (or positron annihilation photons), that it should cover virtually the full volume containing the germanium detectors and that the absolute minimum amount of γ-ray absorbing material should be used within that volume. These requirements are in addition to the need to keep radioactivity to a minimum.

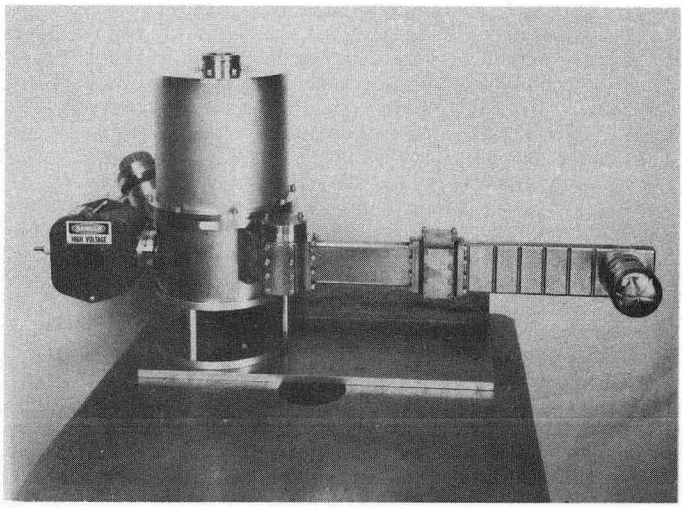

CBB 839-8161

Fig. 11: Photograph of a prototype single detector version of the germanium detector system used in the LBL/UCSB $\beta\beta$ decay experiment. In the final system two detectors are mounted in each vacuum chamber and four dual detector cryostats are employed.

To achieve these objectives the following methods, materials, and techniques have been used:

(i) After a long program of measuring the natural activities in a wide variety of materials, OFHC copper was chosen for use in all structural members.

(ii) The vacuum cryostats for the germanium detectors were made in the form of flat boxes that project through slots in the NaI as shown in Figs. 9 and 10. This geometry minimizes penetration space through the NaI and passive shields and avoids any direct view of the detectors through the shield penetrations.

(iii) Apart from vacuum sealing surfaces (where the detector cap seals to the vacuum chamber in Figs. 11 and 12), very thin (.25 mm) electroplated copper is used for the vacuum box within the volume holding the germanium detectors.

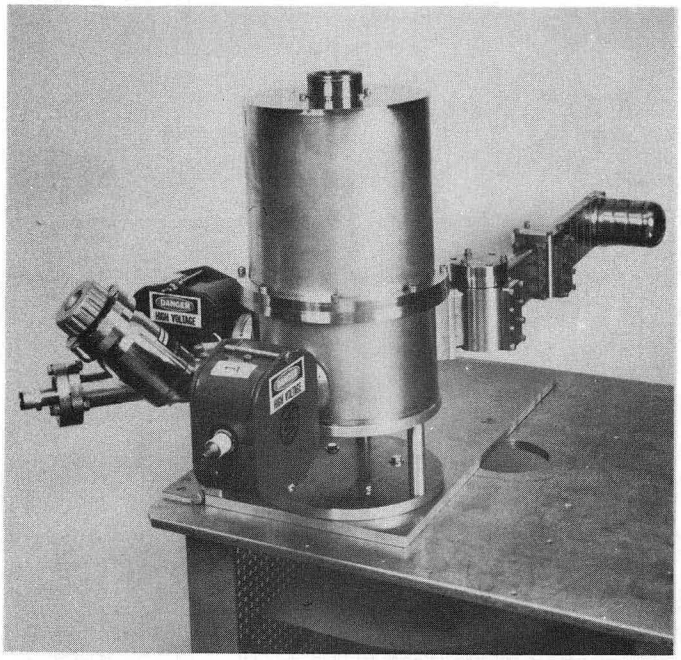

CBB 839-8159

Fig. 12: Same as Fig. 11 but different angle.

Fabrication of these boxes is achieved by plating copper onto an aluminum mandril which has the vacuum sealing ring (1/4" OFHC copper) mounted on it. The plating makes an integral bond to this ring while forming a 1 mm thick plating on the aluminum mandril. Machined depressions in the mandril are used to give the copper skin several ribs that serve to strengthen the chamber. The flat copper faces that will be in the detector volume are machined down to .25 mm thickness leaving the strengthening ribs 1 mm thick. Finally, the aluminum mandril is etched away in a NaOH solution and a brief nickel plating is applied to the copper shell to prevent oxidation of the copper.

The same technique is used to fabricate the .25 mm thick copper vacuum cans (see Fig. 11) that enclose each germanium detector. An O-ring seal is made between this can and the main vacuum chamber. We rely on the vacuum to hold the system together (i.e., no mounting screws or other hardware in the detector chambers).

(iv) Instead of a copper cold finger (an unacceptably thick absorber between the germanium detectors and the NaI shield), a slice of single crystal silicon is used as the cold finger. This material is an inefficient absorber of γ rays, has a thermal conductivity at 77°K that is better than copper and is extremely strong. Its brittle nature means that great care must be exercised in handling it, but these problems are acceptable in this special situation.

(v) Mounting the germanium detectors to the cold finger is accomplished as shown in Fig. 13. Dacron strings, suitably stressed, are used to fasten the germanium detector onto a silicon cylinder, a boron nitride insulator and thence to the cold finger. Difficulties in finding

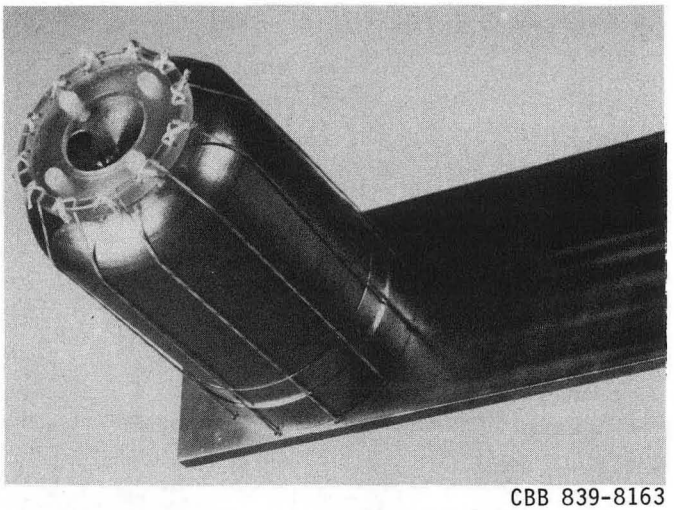

CBB 839-8163

Fig. 13: Photograph showing detector mounting on cold finger.

adequately clean boron nitride led to the use of this arrangement where the silicon cylinder shields the germanium detector from any ^{214}Bi electrons that might be produced by activity in the boron nitride.

(vi) Infrared shielding of the germanium detectors is achieved by metallizing the outer contact of the detectors and all parts (except the BN insulator).

(vii) As stated earlier, very thin (.25 mm) OFHC copper is used for the inside face of the NaI scintillator cans.

(viii) The FET, feedback resistor and capacitor that constitute the front-end elements of the electronic preamplifier are mounted close to each detector. Chip resistors,capacitors and FET's are used to minimize physical size. Fine nickel wires are used to carry the preamplifier connections and the detector bias along the cold finger/vacuum box to the space outside the vacuum shield. All front-end components, including all wires and insulation, were bulk tested for radioactivity prior to use.

C. Special Electronic Features

Appendix A summarizes the sources of background that have the potential to produce spurious counts in the energy regions near 1.5 and 2.0 MeV. Since no natural γ rays are known to occur at precisely the energies of interest (2.041 MeV and 1.482 MeV), we can assume that these counts result almost entirely from higher-energy γ rays interacting in the detector with some of their energy escaping in the form of Compton scattered and/or annihilation-escape photons. Apart from the few cases where these photons are absorbed in dead materials (mainly Cu and Si) in the volume containing the germanium detectors, we expect to reject such events by using signals from the scintillation shield and from the other germanium detectors.

An important uranium decay chain nuclide is ^{214}Bi which decays by β^- emission with an end point of 3.260 MeV. Some of these electrons can essentially duplicate the signals expected from $\beta\beta$ decay; this may well be a major source of background in low background germanium detector systems. Since the vast majority of these electrons must enter through the cylindrical and closed end surfaces of the detectors (the open end is exposed only to silicon in our system and this should be extremely clean) they pass through the thick lithium-diffused n^+ contact (the detectors are made of p-type germanium). Ionization produced in the lithium-diffused regions is collected by diffusion so all signals due to these β particles should be accompanied by a substantial slow component. We have demonstrated that, in fact, this occurs and a slow component reject circuit is included in our system to reject these events.

A second type of electronic pulse shape rejection will also be employed. Appendix B discusses the details of γ-ray absorption in the germanium detectors and the calculated pulse shapes (i.e., shape of the current pulse in the detector) produced by these events. This appendix also discusses the signals that will be produced by single-point events characteristic of $\beta\beta$ decay (electron ranges ~ 1 mm or less). These calculations indicate that recognition of single point events can remove a significant fraction of the γ-ray background in the energy range of interest. To accomplish this, flash digitizers will be used in each germanium detector channel to digitize the detector signals every 20 ns during the charge collection process. As indicated in the analysis of Appendix B, the signal/ noise achieved in this system is adequate to permit rejection of any event containing two or more "prongs" when the main absorption constitutes less than 80% of the energy and when the remaining > 20% is deposited at a radius more than 3 mm away from the main interaction. This technique might be considered a very sophisticated signal filter that provides a limited tracking capability in germanium detectors. Fortunately, we are dealing with sufficiently high energies that noise (in the 20 ns measurements) is not a serious limitation to the technique.

A special technique will also be employed to assist in recognizing the majority of the cosmic-ray generated neutrons that have been produced in and are later captured by the experimental assembly. The incident cosmic-ray particles, muons in this case, will generally be detected by one of the plastic scintillators that surround the assembly. When this detector array fails to report a coincident event in at least one of the other plastic scintillators, we must assume the muon has been captured within the assembly, releasing neutrons in a capture reaction. These neutrons may slow down and in turn be captured within the apparatus, thereby producing a sequence of (n, γ) events that extend over a period of many ms. To recognize such sequences, an interval timer is used to measure the time (to 10 μs resolution) since the most recent "muon capture" event. This information is included in each event record and can be studied when final data analysis occurs.

A very important aspect of this class of experiment should be recognized at the outset. At the most, only a few events of the desired type will be recorded over a period of years. Consequently, a very complete record of each event of interest must be kept for analysis not only by our group but by a whole world of disbelievers. The design of the data acquisition and recording system is intended to satisfy this requirement so that expected questions can be answered when results (positive or negative) are presented.

VI. Conclusion

Double beta decay measurements represent an important application of semiconductor detector technology which presents very special and unique challenges in detector system design and fabrication. The importance of the physics results justifies the new and complex techniques developed; we expect they will inevitably find their way into more general detector applications. The attached bibliography of relevant physics papers should be used by readers interested in obtaining a deeper understanding of the status of $\beta\beta$ decay.

VII. Acknowledgments

We thank the many physicists who have contributed to our knowledge of this subject over the past two years. In particular, conversations with Mark Strovink and Dave Jackson of LBL have been most useful. The UCSB part of our team (David Caldwell, Robert Eisberg, Mike Witherell, and Dave Hale) proposed the project; it is a pleasure to work with them in this challenging experiment.

The work described is directly supported by the Office of High Energy Physics of the Office of Energy Research of the Department of Energy. Much of the work rests on basic support to our detector program provided by the Office of Health and Environmental Research. The Lawrence Berkeley Laboratory is operated for the U. S. Department of Energy under Contract No. DE-AC03-76SF00098.

Reference to a company or product name does not imply approval or recommendation of the product by the University of California or the U. S. Department of Energy to the exclusion of others that may be suitable.

VIII. Bibliography

(1) M. Goeppert-Mayer, Phys. Rev., 48, 512 (1935).

(2) S.P. Rosen and H. Primakoff, Alpha, Beta and Gamma Ray Spectroscopy. K. Siegbahn, Editor, North Holland Press, 1499 (1965).

(3) N. Takaoka and K. Ogata, Z. Naturforsch 21A, 84 (1966).

(4) B. Pontecorvo, Phys. Lett. 26B, 630 (1968).

(5) T. Kirsten, O.A. Schaeffer, E. Norton and R.W. Stoenner, Phys. Rev. Lett. 20, 1300 (1968).

(6) R.K. Bardin, P.J. Gollon, J.D. Ullman and C.S. Wu, Nucl. Phys. A158, 337 (1970).

(7) E. Fiorini, Riv. Nuovo Cimento 2, 1 (1972).

(8) B. Srinivasan, E.C. Alexander,Jr. and O.K. Manuel, Econ. Geol. 67, 592 (1972).

(9) B. Srinivasan, E.C. Alexander,Jr., R.D. Beaty, D.E. Sinclair and O.K. Manuel, Econ. Geol. 68, 252 (1973).

(10) E. Fiorini, A. Pullia, G. Bertolini, F. Capellani and G. Restelli, Nuovo Cimento 13A, 747 (1973).

(11) E.W. Hennecke, O.K. Manuel and D.D. Sabu, Phys. Rev. C11, 1378 (1975).

(12) B.T. Cleveland, W.R. Leo, C.S. Wu, L.R. Kasday, A.M. Rushton, P.J. Gollon and J.D. Ullman, Phys. Rev. Lett. 35, 757 (1975).

(13) A. Halprin, P. Minkowski, H. Primakoff and S.P. Rosen, Phys. Rev. D13, 2567 (1976).

(14) D. Bryman and C. Picciotto, Rev. Mod. Phys. 50, 11 (1978).

(15) F.T. Avignone, III and Z.D. Greenwood, Nucl. Inst. and Meth. 160, 493 (1979).

(16) M.K. Moe and D.D. Lowenthal, Phys. Rev. C22, 2186 (1980).

(17) V.A. Lubimov, E.G. Novikov, V.Z. Nozik, E.F. Tretyakov and V.S. Kosik, Phys. Lett. 94B, 266 (1980).

(18) Weak Interactions as Probes of Unification. AIP Conference Proceedings No. 72, (1981).

(19) H. Primakoff and S.P. Rosen, Ann. Rev. Nucl. Part. Sci. 31, 145 (1981).

(20) N.A. Wogman, IEEE Trans. Nucl. Sci. NS-28, 275 (1981).

(21) W.C. Haxton, G.J. Stephenson,Jr. and D. Strottman, Phys. Rev. Lett. 47, 153 (1981).

(22) E. Fiorini, Phil. Trans. R. Soc. Lond. A304, 105 (1982).

(23) E. Bellotti, E. Fiorini, C. Liguori, A. Pullia, A. Sarracino and L. Zanotti, Phys. Lett. 121B, 72 (1983).

(24) Science Underground, AIP Conference Proceedings No. 96, Chpt. VIII (1983).

Appendix A: Background Sources

1. Natural Terrestrial Activities.

The major natural terrestrial activities are those associated with the uranium and thorium decay chains and ^{40}K. In our case, the uranium and thorium decay chains are the dominant concerns. These chains involve a combination of α decays (8 for the U- chain and 6 for the Th- chain) interspersed with β^- decays. The dominant parent nuclide of the U-chain present in many newly processed materials ("pure" metals, alloys, ceramics and plastics) is ^{226}Ra decaying with a half life of 1600 years through a sequence of relatively short-lived nuclides to the stable end member of the chain, ^{206}Pb. Other newly processed materials contain only the uranium members of the U-chain, ^{226}Ra being blocked by the long half life (8×10^4 years) of ^{230}Th in the time scale of interest here. The parent of the Th-chain is ^{232}Th, decaying with a half life of 1.4×10^{10} years through a sequence of relatively short-lived nuclides to ^{208}Pb. Newly processed materials, such as aluminum and its alloys, may contain only the thorium members of this chain (^{232}Th and ^{228}Th), a circumstance which leads to dramatic changes in

activity levels throughout approximately the first ten years following processing. Alternatively, engineering materials which undergo little or no chemistry during processing (some glasses, ceramics, and plastics that have fillers) may contain both U- and Th-chains in equilibrium, as reflected by the abundances of these nuclide families in raw materials.

Background in our detectors can be produced by α and β particles emitted in the decay chains or by γ rays emitted during the deexcitation of excited levels of daughter nuclei. Clearly the worst case would occur if activity existed within the detectors themselves and if the energy deposition corresponded exactly to the $\beta\beta$-decay lines. The extreme measures adopted in purifying germanium plus the purification involved in forming single crystals should result in virtually no natural activity except for the $\beta\beta$ decay of ^{76}Ge. Furthermore, since the detectors would truly measure the energy involved in any internal radioactive decay processes (i.e., with no degradation of signals), any α or β decays whose energy did not precisely (within 2 keV) equal the 2.041 MeV or 1.482 MeV line of interest would be rejected on energy considerations. Since the γ's produced by α and β decays in the detector are essentially simultaneous with the main decay, signals due to them are also easily rejected.

These considerations suggest that the main sources of interfering background are decays that occur in materials near the germanium detectors where only part of the total energy involved in the decay process reaches the detector. Fortunately, except for the open end of the coaxial detector, charged particles (α or β) enter the detector through the lithium-diffused outside n^+ contact and the slow signal component diffusing in from this region can be detected and consequently rejected. The open end of the detector is more sensitive to these events; for this reason we have chosen to protect the open end with single crystal silicon which should be (and by test is) extremely clean.

We are, therefore, left with background mainly due to high-energy γ rays entering the detector and interacting by either Compton scattering or pair production (or a combination), leaving a portion of their energy in the detector such that the signal amplitude mimics the events of interest to us. Focusing for the moment on the 2.041 MeV case, the interfering incident γ rays must exceed this energy; the excess energy will leave the germanium detector and, hopefully, be detected by either the NaI shield or another germanium detector. Despite the small amount of other material we have in our counting chamber, a finite though extremely small probability exists for the escape photon to be absorbed in this dead material and not reach the active reject detectors. (Note: the 0.8 mm thick lithium-diffused outer germanium detector contact is the largest absorber present in our system, but slow signal components from this material should provide a reject mechanism for events whose energy is deposited in these regions).

From these arguments it is clear that the γ rays with energy greater than 2.041 MeV produced by natural radioactive nuclides are the most serious candidates to produce background that will interfere with the 2.041 MeV $\beta\beta$ decay events. Table 2 summarizes the natural activities that produce β particles and γ rays whose energy exceeds 2.041 MeV.

Table 2: Natural Terrestrial Activities producing > 2 Mev

Decay Series	Nuclide	Betas		γ-rays*	
		Endpoint keV	Betas/ 100 decays	Energy keV	Photons/ 100 decays
Uranium	Pa-234 m	2290	0.6	—	—
"	Bi-214	3260	19	2053(609)	.07
				2110(609)	.10
				2119(609)	1.30
				2204	5.30
				2294	.03
				2448	1.65
				3054	.02
Thorium	Ac-228	2180	10	—	—
	Bi-212	2270	40	—	—
	Tl-208	2380	.01	2614(583)	23
				2614(860)	4
				2614(510/ 583)	8

*Values in parentheses are γ-rays coincident with the listed γ-ray.

Also indicated in this table are cases where high-energy γ rays are accompanied by other (essentially) coincident γ rays. In these cases, the rejection system becomes even more effective because the coincident γ ray may also be detected to provide a rejection tag. This applies, for example, to an important potential interfering γ ray--that of ^{208}Tl at 2.614 MeV. Here the coincident γ rays as well as the γ rays escaping from a germanium detector provide rejection possibilities even though the signal in the germanium detector might mimic the 2.041 MeV event of interest.

The presence of airborne ^{222}Rn (parent of potentially interfering high-energy radiation from the U-chain) may require the entire apparatus to be operated in a gas-tight enclosure filled with Rn-free gas. This problem would be expected to be most severe at an underground laboratory suggesting that selection of such an experimental site must include the parameter of low radioactivity in the surrounding rock formation.

The situation becomes more complicated if we consider potential interference with the 1.482 MeV peak. Additional γ rays must be considered but the same general arguments apply and we will not consider the situation in detail.

2. Cosmic-Ray Induced Activities

Cosmic rays passing through materials in the detector assembly (particularly the lead shield) cause γ-ray background by several mechanisms, the most troublesome of which is the production of fast neutrons that subsequently are moderated and captured by materials close to (or inside) the detector. Neutron capture in most materials produces nuclei with large (up to ~ 10 MeV) excitation; deexcitation of these nuclei results in many "prompt" high energy γ rays. Thermalizing the neutrons may take some time (up to ~ 100 ms), so the γ rays resulting from passage of a cosmic ray may be delayed by a substantial time--too long to be vetoed by a prompt reject gate of any

reasonable length. Relatively long-lived radioactive nuclei (β^- emitters) may be produced and they will constitute a further background source. Fortunately, such long-lived isotopes generally produce relatively low-energy radiation. It is also fortunate that the high excitation energy produced by neutron capture will usually result in "prompt" cascades of γ rays so the rejection mechanism again becomes more effective since rejection can be accomplished by detecting any γ ray in the cascade. To guard against cosmic rays, we will use reject detectors to tag events that immediately follow passage of a cosmic ray; the use of a timer recording the interval between recorded events will also permit later examination of the time relationship between events, over the range 10 μs to 100 ms.

Table 3: Neutron Capture γ Rays

Element	Capture σ barns	γ-Ray Energy	γ-Ray per 100 Captures
H	0.33	2223	100
B	755 (n, α)	477	95
C	0.0034	1262	29.5
		3684	32.1
		4945	67.6
N	0.075	1885	22
		2062	3.7
		2157	3.6
		2174	2.6
		2357	4.4
		2521	6.8
		2831	2.2
		3014	0.9
O	0.00027	871	100
		1088	82
		2184	82
		3271	18
F	0.0095	215	80
		582	13
		2453	10.2
		2528	8.4
		2602	9.0
		2632	5.4
		2662	6.4
		2683	7.8
		2699	4.5
		3017	4.0
		3052	5.2
		3074	9.2
Na	0.40	472	60
		871	22
		2027	17
		2057	1.2
		2124-2505(8)	17.1
		2518	14.8
		2594-3026(7)	25.9
		2863	10.2
Si	0.16	2030	2.25
		2093	21.5
		2158-3054(10)	11.3
		2426	3.0
Ni	4.43	465	13.0
		2093-3042(15)	6.4
Cu	3.79	278	32.7
		2136-3054(13)	5.0
Ge	2.30	596	33.1
		2031	0.26
		2074-2953(8)	2.5
		3028	39.0
I	6.20	134	8.4
		443	4.4
		2207	0.6
		2938	0.2
Tl	3.40	349	2.6
		2111-2859	1.4
Pb	0.17	6736	5.0
		7368	94.1

Table 3 shows the important γ rays expected to be produced by neutron capture in most of the elements present in the detector assembly including germanium, silicon, boron nitride (small quantity), sodium iodide, copper, lead and various plastics (H,C,N,O). We see that many high-energy γ rays are produced; the "above ground" background (1) shown in Fig. 7 probably results from stacking of Compton distributions produced in the germanium detector by these various γ rays. The rejection mechanisms employed in our system are expected to drastically reduce the background due to these sources. However, we also expect to move the system to an underground laboratory to reduce cosmic rays by a large factor after initial tests in our LBL low background facility.

A particularly difficult background problem may be caused by neutron capture in ^{76}Ge to produce ^{77}Ge and ^{77m}Ge. ^{77}Ge decays by β^- emission (highest end point energy = 2.2 MeV, half life = 11 hrs), but the β^- emission is accompanied by emission of γ rays up to about 250 keV. Therefore, rejection of many of the ^{77}Ge decay signals can probably be accomplished. ^{77m}Ge is a more difficult case. It decays largely by β^- emission (end point ~ 2.9 MeV) with a 54 sec half life to the ground state of ^{77}As. Consequently, no accompanying γ rays occur and our rejection methods fail. Fortunately, the cross-section for neutron capture in ^{76}Ge is very low; we estimate that only 0.15% of all neutron capture events in natural germanium produce ^{77m}Ge nuclei that decay with pure β^- emission. Despite this low probability, this background source is a clear reason for working in an underground laboratory where cosmic rays are largely eliminated.

Appendix B: Detector Pulse Shape Discrimination

We plan to use a simple slow component reject technique to eliminate events producing ionization in the 0.5-0.8 mm thick lithium-diffused n^+ contact surrounding most of the outer surfaces of the germanium detectors.

A more sophisticated fast pulse shape discrimination system will be used to select events where all the energy deposition occurs in a small region (~ 1 mm space) as compared with events where energy deposition is distributed. This technique will be implemented by digitizing the "current signal" from the detector every 20 ns. Differentiation of the integrated charge signals appearing at the output of the germanium detector preamplifiers provides the current signal. For our detectors, the charge collection takes up to about 400 ns, so 20 samples are stored with other data on relevant signals. The shape of the "current signal" depends on the radial distribution of the initial charge deposition by a γ ray; therefore, ideally, we are able to distinguish those γ-ray events where interactions occur at multiple points from the $\beta\beta$ decay events where the total energy deposition occurs in a small volume (~ 1 mm in size).

While this basic shape discrimination principle is easy to understand qualitatively, it is very difficult to determine the quantitative reduction of γ-ray background that will result from its use. To make an estimate of this we have generated a set of computer simulations of various aspects of the process. The steps taken are as follows:

(i) We have developed a Monte Carlo simulation of γ rays of various energies entering the face of our coaxial detectors at random radii in an axial direction. This indicates that a > 50% reduction in background (for the 2.041 MeV region) can be achieved if we assume that the shape discrimination method can recognize events where more than 20% of the energy is deposited at a radius 3 (or more) mm from the main absorption. The axial orientation of γ rays is a worst case situation and some further background reduction can be expected for the random orientations that will be characteristic of the background γ rays in our system. The spectrum produced by the ^{208}Tl 2.6 MeV γ ray is shown in Fig. 14. This is a calculated spectrum; the experimentally measured spectrum closely agrees with this, giving us confidence in the Monte Carlo calculations.

(ii) The electric field distribution in the coaxial region of one of our detectors is shown in Fig. 15.

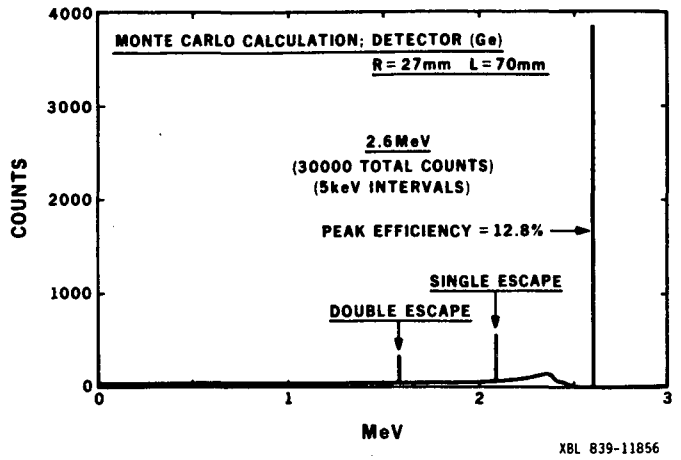

Fig. 14: Calculated spectrum for ^{208}Tl γ ray at 2.6 MeV using a coaxial germanium detector (55 mm dia, 70 mm length). Measured spectrum agrees with calculation.

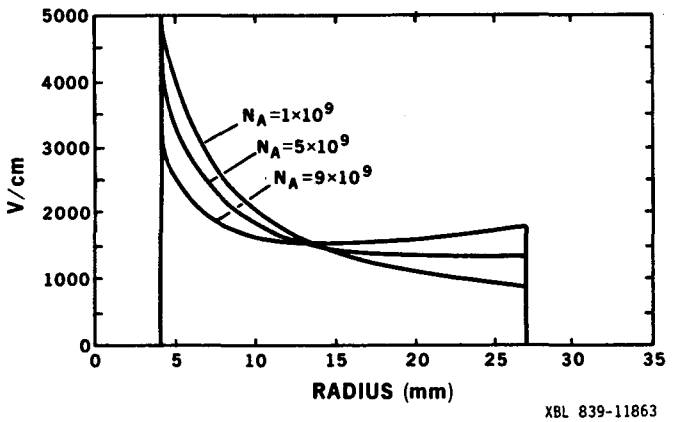

Fig. 15: Radial distribution of electric field for a coaxial detector (inner radius 4 mm, outer radius 27 mm). Curves are shown for acceptor concentrations N_a = 1, 5 and 9 x $10^9/cm^3$. This is typical of the longitudinal variation in our detectors.

The various curves correspond to the impurity concentrations that exist along the length of one of our detectors. The signal shape produced by events occurring at a fixed radius would be expected to be almost independent of the impurity concentration if the electric field exceeds 1000 V/cm at all points.

(iii) From the electric field distribution and the relationship between hole and electron mobilities as a function of electric field, we can calculate the pulse shape to be expected for events occurring at different radii. Figure 16 shows representative single point absorption examples, and the (small) effects due to variable impurity concentrations along the length of the detector are also illustrated. Note that these shapes show the integrated charge; the sampled differential of these shapes will be stored in our system. Also illustrated is an event where the energy deposition is 80% at a radius of 18 mm and 20% at a radius of 15 mm. Figure 17 shows a complete set of pulse shapes for events located at 4 mm radial intervals.

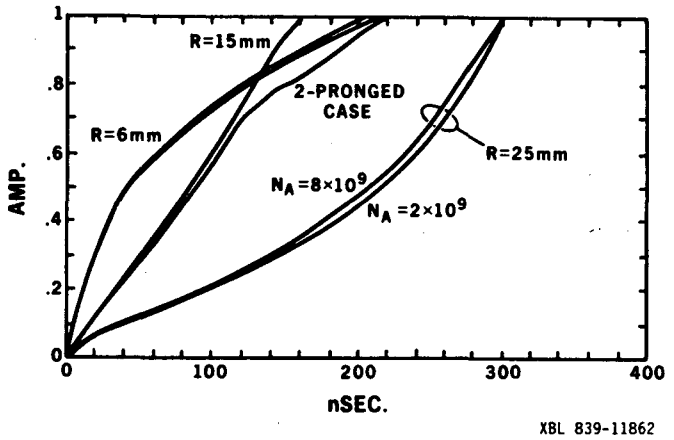

Fig. 16: Integrated charge pulse shapes for events at the indicated radii and impurity concentrations. A 2-pronged event is shown for comparison with the other single point events.

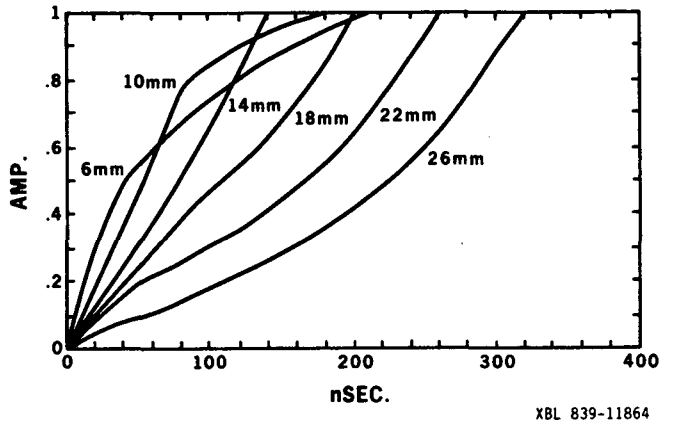

Fig. 17: Complete map of single point event pulse shapes for radial intervals of 4 mm.

(iv) A matching program has been developed that provides an automatic way of filtering multi-pronged events from single point events. The following steps are executed by this program:

a) A map is constructed of all single point event current pulse shapes for radial steps of 1 mm.
b) A test 2-pronged event (or 3-pronged) is simulated with various percentage energy distributions in the prongs and the current pulse shape is calculated.
c) The deviations between the 2-pronged event and each of the single point shapes is computed at each 20 ns interval. For each radius of the single point events, the computer then calculates Σ (deviation)^2 over the range 0 to 400 ns. The value of this quantity is plotted against the radius of the reference shape.

Figure 18(a) shows the result when the event leaves its energy deposition at one radius (18 mm). The curve of Σ (deviation)^2 is relatively flat but with a very sharp dip at the radius where the test event exactly matches one of the map event radii. In Fig. 18(b) the same test is performed, but a typical

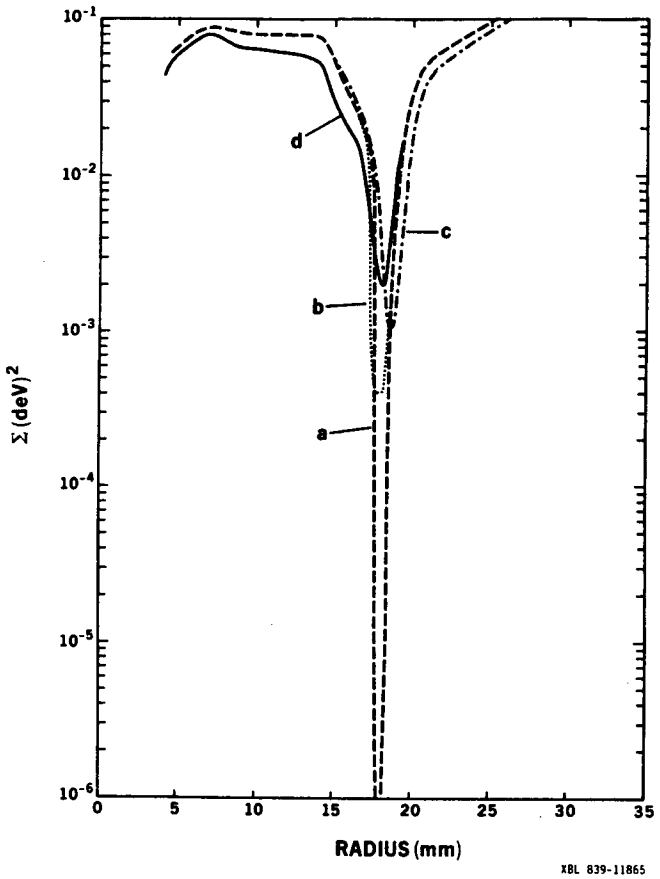

Fig. 18: a) A plot of Σ(deviation)^2 of a single point event at r = 18 mm where the deviation is measured with respect to each of the map shapes at 1 mm radial intervals.
b) Repeat of (a) but with typical noise of 18 keV FWHM added to signals.
c) Repeat of (a) but with the energy distributed 50% at 18 mm and 50% at 19 mm radius.
d) Repeat of (a) for a 2-pronged event--split with 80% of energy at r = 18 mm and 20% at r = 15 mm.

electronic noise spread is introduced on each 20 ns measurement point of the test event shape (assuming a full pulse amplitude of 2 MeV). The dip in the curve at 18 mm radius is shallower than in curve (a) as might be expected. Remembering that the $\beta\beta$ decay event of interest spreads its energy over a region roughly 1 mm in size, we demonstrate in Fig. 18(c) the effect of distributing the test event energy equally at two points 1 mm apart. Again the dip in the curve at 18-19 mm is shallower; this curve was generated with no noise; it is obvious by comparing Fig. 18(b) and (c) that the spreading effect of the 1 mm energy distribution substantially exceeds the spreading effect of the noise present in our measurements.

The final result shown in Fig. 18(d) shows the effect of trying to match a 2-pronged test event where the charge distribution is 80% at 18 mm radius and 20% at 15 mm radius. This curve clearly shows asymmetry and the dip at 18 mm is not as pronounced as in Fig. 18(c). Therefore, with the realistic assumptions of the model, it is clear that a relatively simple criterion can be established for distinguishing such events that occur in the coaxial portion of our detectors (which represent a large fraction of the volume). We believe that the method can be extended to cover the closed end of the detector but no work has yet been done on this problem.

This "least squares technique" is not considered to be an optimum selection method but, even in its present form, we feel that it can be an automatic filter selecting events for visual inspection of the pulse shape data. Features not recognized by this simple automatic filter can be seen visually, so our assumption that we can recognize events where the energy deposition (~ 2 MeV) is split 80% at one radius and 20% at least 3 mm different in radius seems to be a safe one.

This report was done with support from the Department of Energy. Any conclusions or opinions expressed in this report represent solely those of the author(s) and not necessarily those of The Regents of the University of California, the Lawrence Berkeley Laboratory or the Department of Energy.

Reference to a company or product name does not imply approval or recommendation of the product by the University of California or the U.S. Department of Energy to the exclusion of others that may be suitable.

TECHNICAL INFORMATION DEPARTMENT
LAWRENCE BERKELEY LABORATORY
UNIVERSITY OF CALIFORNIA
BERKELEY, CALIFORNIA 94720